

The following article appeared in Journal of Advanced Dielectrics 5(4): 1550034 (2015); and may be found at:  
<https://doi.org/10.1142/S2010135X15500344>

This is an open access article under the Creative Commons Attribution 4.0 International (CC BY 4.0) license

<http://creativecommons.org/licenses/by/4.0/>

## BiFeO<sub>3</sub> codoping with Ba, La and Ti: Magnetic and structural studies

O. García-Zaldívar<sup>\*,†,¶</sup>, S. Díaz-Castañón<sup>\*,§</sup>, F. J. Espinoza-Beltrán<sup>†</sup>,  
M. A. Hernández-Landaverde<sup>†</sup>, G. López<sup>‡</sup>, J. Faloh-Gandarilla<sup>\*</sup>  
and F. Calderón-Piñar<sup>\*,†</sup>

<sup>\*</sup>Facultad de Física — Instituto de Ciencia y Tecnología de Materiales  
Universidad de La Habana, San Lázaro y L  
Vedado, La Habana 10400, Cuba

<sup>†</sup>CINVESTAV-Unidad Querétaro, Libramiento Norponiente No. 2000  
Real de Juriquilla, Querétaro, Qro. 76230, México

<sup>‡</sup>Instituto Latino-Americano de Ciências da Vida e da Natureza  
Universidade Federal da Integração Latino-Americana, (ILCVN-UNILA)  
Avenida Tancredo Neves, PTI, Bloco 6  
CEP: 85866-000 — Foz do Iguaçu — Parana, Brazil

<sup>§</sup>División Materiales Avanzados  
Instituto Potosino de Investigación Científica Tecnológica  
San Luis Potosí, CP 78216, México

<sup>¶</sup>osmany.garcia@gmail.com; ogz@imre.oc.uh.cu; osmany.garcia@cinvestav.mx

Received 19 October 2015; Revised 9 November 2015; Accepted 13 November 2015; Published 28 December 2015

Conventional solid state reaction method, from oxides and carbonates, was employed to prepare bismuth (Bi)-based multiferroic systems. The undoped BiFeO<sub>3</sub> (BFO) and the codoped system with Ba, La and Ti (Bi<sub>1-x</sub>Ba<sub>x</sub>Fe<sub>1-y</sub>Ti<sub>y</sub>O<sub>3</sub>, Bi<sub>1-x-z</sub>Ba<sub>x</sub>La<sub>z</sub>Fe<sub>1-y</sub>Ti<sub>y</sub>O<sub>3</sub>) with  $x, y, z = 0.1$  were prepared stoichiometrically and sintered at two different temperatures. The structural and magnetic properties were investigated at room temperature. XRD measurements confirm the obtaining of the rhombohedral perovskite structure of the BFO family system. For the undoped system, some reflections of undesired phases are present for two different sintering temperatures, while for the doped system only one phase is present for both temperatures. The magnetic characterization at room temperature revealed remarkable differences between the ceramic samples. The results show that for undoped BFO system, spontaneous magnetization is not observed at room temperature. Nevertheless, in doped one, a well-defined ferromagnetic behavior is observed at room temperature, possible, due to the suppression of the spatially modulated spin structure of BFO promoted by the reduction of the rhombohedral distortion and the weakening of the Bi–O bonds. The XPS results confirm the presence of oxygen vacancies and the coexistence of Fe<sup>3+</sup> and Fe<sup>2+</sup> in all the studied samples. Calorimetric measurements reveal that the dopant incorporation has not a direct effect in Néel temperature but possibly yes in ferroelectric-paraelectric transition.

**Keywords:** Multiferroics; XPS; magnetic; bismuth ferrite BiFeO<sub>3</sub>.

### 1. Introduction

The study and characterization of ferroic materials (those with ferroelectric, ferromagnetic or ferroelastics order) is of great importance because of the large variety of applications derived from its properties.<sup>1–6</sup> Ferroelectric systems can be used in industrial applications such as next-generation sensors, transducers, micro-electromechanical systems, nonvolatile random access memories, high energy density capacitors, among others.<sup>7,8</sup> While, materials with magnetic ordering can be used in data storage devices, as a component in devices for converting mechanical energy into electrical energy and

many other industrial applications.<sup>9</sup> There is growing interest in the study, characterization and sintering of new multiferroic materials (those in which coexist in a single phase and the same temperature range, ferroelectric and ferromagnetic properties) in recent years<sup>10–13</sup> because of the impact they would have on the development of new applications. The availability of materials in which magnetic and electric order coexist opens a window of possibilities for the development of new technologies. In 1973, Wood and Austin<sup>14</sup> proposed 15 different applications for these materials. Some of them are magnetoelectric data storage devices, spin wave

<sup>¶</sup>Corresponding author.

generators, amplifiers and amplitude modulators. All of which has prompted the scientific community to engage in the study of these systems.

One of the difficulties in the development of applications based on multiferroics materials is related to obtaining multiferroics systems where, in the same phase, the ferroelectric and ferromagnetic properties in a temperature range above room temperature coexist. In 2000, a report by Nicola Hill<sup>15</sup> discusses the conditions that must exist in a material so that it possesses ferroelectric and ferromagnetic properties. It is noted that in the best known ferroelectrics, with perovskite structure, the transition element is in 3d<sup>0</sup> state (unoccupied level, such as Ti<sup>4+</sup>), while in the best known ferromagnetic systems with perovskite structure, the transition element is in 3d<sup>n</sup> state (partially occupied level, such as Mn<sup>3+</sup>). Both elements are located in the B site of the perovskite structure in PbTiO<sub>3</sub> and BiMnO<sub>3</sub> systems. So, in principle, in perovskite systems, the conditions that optimize ferroelectricity are opposed to that optimize ferromagnetism. However, there are materials which coexists in the same phase, the magnetic and electrical order simultaneously. Nevertheless, in many of them, the magnetic ordering stabilize at temperatures below 0°C.<sup>15</sup>

One of the most promising multiferroics systems is bismuth ferrite (BFO), having a remnant polarization as a thin layers over 60 μC/cm<sup>2</sup>,<sup>13,16</sup> higher than previously reported for based ferroelectrics PZT systems. It is characterized by the high Curie (T<sub>C</sub> = 1103 K) and Néel temperatures (T<sub>N</sub> = 643 K).<sup>17</sup> From the magnetic point of view, BFO exhibits a canted spin arrangement between near Fe<sup>3+</sup> ions leading to weak ferromagnetism. Nevertheless, the system is antiferromagnetic at macroscopic level due to its spiral spin structure with a modulation length of 62 nm.<sup>18</sup>

This system presents three main difficulties that prevent its use for different applications: (i) it is difficult to obtain materials free of impurities by conventional methods. The phase BFO is thermally unstable at the sintering temperature, forming other stable undesirable phases; (ii) this system has a high electrical conductivity conspiring with its ferroelectric properties; (iii) its antiferromagnetic order at room temperature prevents their use in certain applications (such as data storage).

These difficulties could be minimized or even eliminated with the modification of this system with rare earths (such as lanthanum), alkaline elements (such as barium, calcium, cadmium) or transition elements with level 3d unoccupied (such as titanium Ti<sup>4+</sup>). Studies so far show that it is possible to improve the electrical and/or magnetic properties by doping these materials with some of these elements.<sup>11,12</sup>

The modified systems with barium are among the most investigated and in which the best results have been achieved.<sup>11,12,19–21</sup> However, these substitutions are made, generally, regardless the electric imbalance caused by the valence difference between Bi<sup>3+</sup> and Ba<sup>2+</sup>. This electric imbalance can be compensated during synthesis, by creating

defects such as the formation of spurious phases, creating oxygen vacancies and/or the reduction of Fe<sup>3+</sup> to Fe<sup>2+</sup>. On the other hand, in order to reduce or controlling the formation of such defects, electrical neutrality can be achieved, stoichiometrically, by codoping the materials with adequate quantities of other elements that compensate the electric imbalance created by Ba substitution (i.e., codoping the material with Zr<sup>4+</sup> or Ti<sup>4+</sup>).

The aim of the present work is to study the influence of codoping with Ba and Ti and with Ba, La and Ti in the structural and magnetic properties of modified BFO. In this paper, we will discuss the possible causes of the magnetic properties improvement in doped BFO system.

## 2. Experimental Procedure

Traditional ceramic method was used to obtain the ceramics samples. The nominal composition for the pure and BFO modified ceramics are Bi<sub>(1-x-z)</sub>Ba<sub>x</sub>La<sub>z</sub>Fe<sub>(1-x)</sub>Ti<sub>x</sub>O<sub>3</sub> (x = 0 and z = 0 (BFO); x = 0.1 and z = 0 (BBFT); x = 0.1 and z = 0.1 (BBLFT)), considering that Ba and La partially replace the bismuth (Bi) in the A sites of the perovskite structure and Ti partially replace the Fe in the B site of the structure.

The corresponding high purity precursor oxides (Bi<sub>2</sub>O<sub>3</sub>: 99.9%, BaCO<sub>3</sub>: 99%, La<sub>2</sub>O<sub>3</sub>: 99.9%, TiO<sub>2</sub>: 99.5%, Fe<sub>2</sub>O<sub>3</sub>: 99.0%) were ball-milled for 2 h, pressed and calcined at 700°C for 1 h. The calcined powders were re-milled for 2 h, pressed and sintered at 850°C and 900°C during 1/2 h in air in order to choose the adequate sintering temperature. No excess Bi<sub>2</sub>O<sub>3</sub> was added during the process.

Phase identification, at room temperature, was performed by X-ray powder diffraction (XRD) on a RIGAKU (Dmax 2100) diffractometer using Cu Kα radiation in a 2θ range from 10° to 70°, a step scan of 0.02° and a integration time of 0.4 s. Scanning electron microscopy (SEM) images of the ceramics samples were performed using a Philips XL30 ESEM scanning electron microscope. The images were recorded in secondary electron (SE) mode and back scattering electron (BSE) mode over fractured samples. The Raman scattering spectra were recorded at room temperature using a Dilor (LabRam II) micro-Raman spectrometer. The measurements were performed with a laser spot size of 1 μm and an excitation line of 488 nm.

Differential scanning calorimetry (DSC) was carried out in a Mettler Toledo DSC822e calorimeter in the temperature range from 300 K to 1000 K in air. X-ray photoelectron spectroscopy (XPS) was performed in a XPS110 Thermo-Fisher-VG Instrument with a AlKα source (1486.7 eV).

The magnetic properties, in a temperature range between 5 K and 300 K, of the samples were measured using an Evercool Physical Properties Measurement System (PPMS P525 Quantum Design). The maximum applied field used in the measurements was 30 kOe.

### 3. Results and Discussion

Figure 1 shows the X-ray diffraction patterns of the samples sintered at 900°C. The analysis revealed the formation of the BFO rhombohedral perovskite structure in all the studied samples. In BFO-900 sample, some remnants of undesired phases of mixed iron Bi oxides are present (identified as \* in the graphs), while in the BBFT-900 and BBLFT-900 undesired phases can be detected. The minority phase was identified as  $\text{Bi}_{25}\text{FeO}_{40}$  according to pdf # 00-046-0416 from ICDD, that can be easily eliminated leaching the samples in  $\text{HNO}_3$ .<sup>22</sup> The identification of crystallographic family of planes, corresponding to BFO phase, according to (pdf # 00-020-0169 from ICDD) are presented as well. It is worth to note here that the thermal stability of the phase of doped samples was corroborated with the diffraction pattern performed in samples sintered at 850°C (not shown here for simplicity), obtaining the same results.

The results of semiquantitative analysis of the phases and cell parameters in all samples are shown in Table 1. For the quantification, whole pattern fitting (WPF) method was used with the software JADEv9 (MDI). As can be seen, the  $\text{Bi}_{25}\text{FeO}_{40}$  content is around 5% in the undoped sample, while in doped ones this phase could not be quantified because, if is present, lies below the sensibility of the XRD technique.

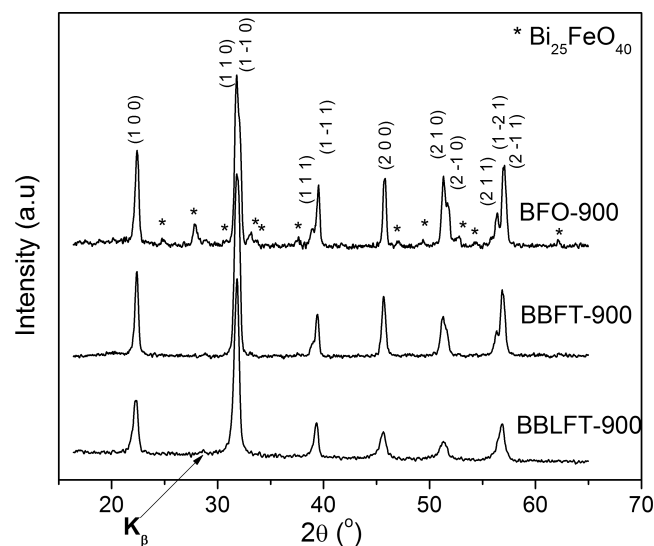


Fig. 1. X-ray diffraction patterns at room temperature of BFO-900, BBFT-900 and BBLFT-900.

Table 1. Phase content in % and cell parameters.

Phase	%	$a_R$ (Å)	$\alpha_R$
BFO	94.8	3.964	89.43
$\text{Bi}_{25}\text{FeO}_{40}$	5.2	—	—
BBFT	100	3.971	89.49
BBLFT	100	3.974	89.67

On the other hand, even though the size difference between  $\text{Bi}^{3+}$  (1.38 Å) and  $\text{Ba}^{2+}$  (1.61 Å) is significant, no remarkable difference is observed in the cell dimensions between undoped and doped samples. This could be as a result of the simultaneous substitution, even though the size difference between  $\text{Ti}^{4+}$  (0.61 Å) and  $\text{Fe}^{3+}$  (0.55 Å) is lesser than that of the A site cations. The parameter  $a_R$  increases slightly, while  $\alpha_R$  tend to 90°, approaching to the cubic structure with the dopants incorporation. Therefore, it could be concluded that the dopants incorporation reduce the rhombohedral distortion introduced by the lone pair  $6s^2$  of the  $\text{Bi}^{3+}$ .

Figure 2 shows SEM images of the ceramic samples in SE mode (BFO-900: Fig. 2(a), BBFT-900: Fig. 2(c), BBLFT-900: Fig. 2(e)) and BSE mode ((BFO-900: Fig. 2(b), BBFT-900: Fig. 2(d), BBLFT-900: Fig. 2(f)). There is a huge difference in the grain morphology between the doped and undoped samples. The undoped samples are formed by large grains with poorly defined grain boundaries. As can be seen there is a continuous reduction of grain size with the dopant incorporation. This reduction could be related to the fact that the dopant ion acts as a point defect (limiting substance) that inhibit the diffusion process during the grain growth.

The segregation of impurity phases to the grain boundaries in BFO-900 sample, is clearly observed in Fig. 2(b). Lighter zones around the grains are related to the Bi-rich phase. Interestingly, in the BBFT-900, although this phase could not be detected by X-ray diffraction, some lighter regions at the boundaries of some grains reflects the minority presence of  $\text{Bi}_{25}\text{FeO}_{40}$  in this system (Fig. 2(d)).

Thermal analysis results of the studied samples are shown in Fig. 3. Two anomalies can be observed, except for BBLFT-900, in the middle and high temperature regions. The first anomaly, around 643 K for BFO-900 and BBFT-900 can be attached to Néel temperature. That is, dopant incorporation do not have a direct effect in magnetic transition temperature. The lack of anomaly around  $T_N$  for BBLFT-900 sample could be related to a weakening of cooperative long range magnetic interactions promoted by La incorporation, provoking a low heat transfer around the transition temperature.

On the other hand, ferroelectric transition is highly affected by dopant incorporation. The anomaly around 1103 K observed in BFO-900 system is related to the Curie temperature. For the doped samples,  $T_C$  continuously shift to lower temperatures with dopant incorporation: around 1005 K for BBFT-900 and 912 K for BBLFT. It is a well established fact that the rhombohedral distortion introduced by the lone pair  $6s^2$  of the  $\text{Bi}^{3+}$  and the strong hybridization between Bi ( $6s^2 6p^3$ ) and O ( $2s^2 2p^4$ ) are responsible for the ferroelectric ordering of BFO family system. Hence, a reduction in ferroelectric transition temperature could be a reflection of a weakening in the Bi–O bonds. This supposition could be supported by the reduction of the rhombohedral distortion, detected by X-ray diffraction with the dopant incorporation.

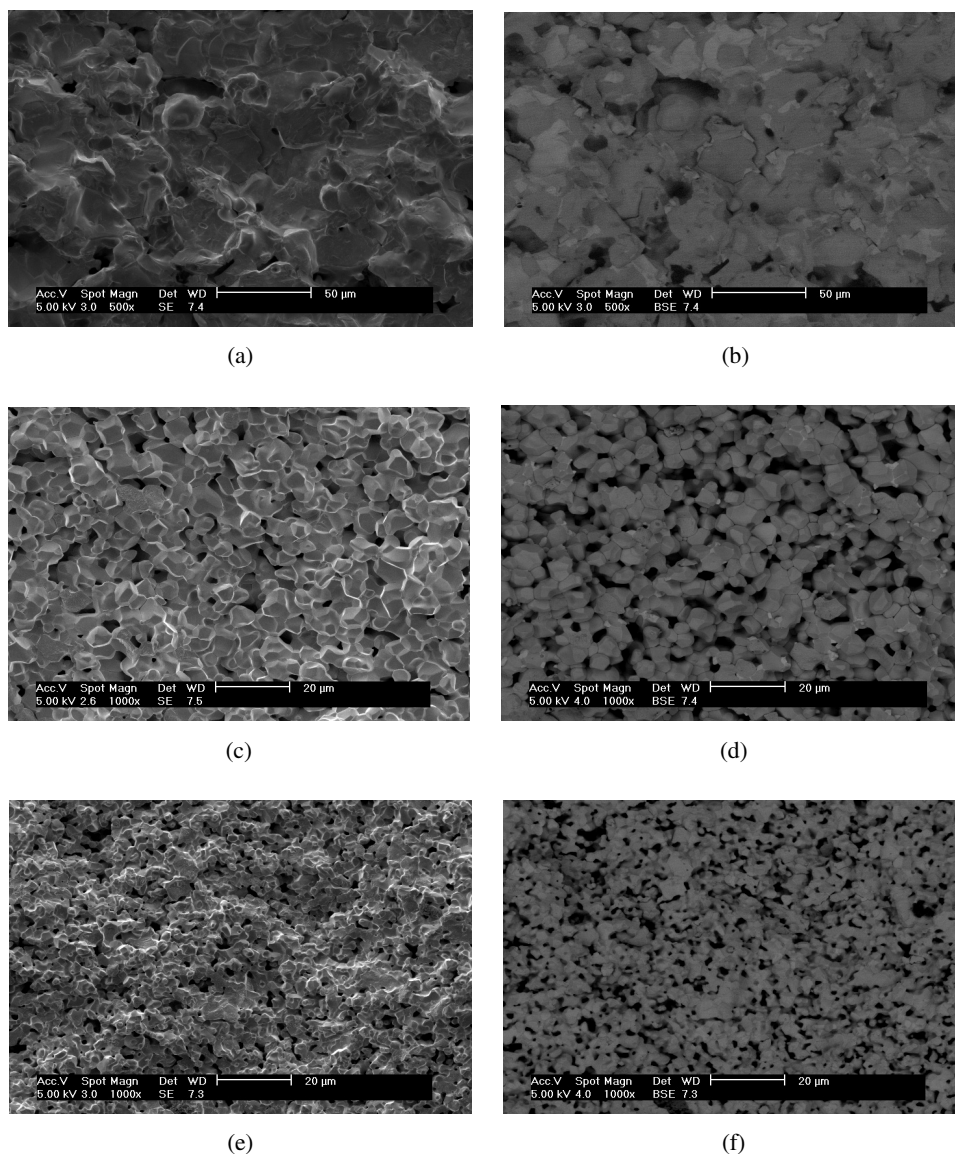


Fig. 2. Scanning electron micrograph of (a) BFO-900 (SE), (b) BFO-900 (BSE), (c) BBFT-900 (SE), (d) BBFT-900 (BSE), (e) BBLFT-900 (SE) and (f) BBLFT-900 (BSE).

Figure 4 shows the Raman spectra recorded for all the studied samples. Typical wide peaks, of polycrystalline system, due to thermal motion and lattice disorder are observed. Note that the modes are less resolved due to increase of peaks widening with dopant incorporation. The assignments of Raman modes is highly contradictory in the literature for BFO system. In the present work, mode assignments were made according to theoretical and experimental works, in single crystal, carried out by Hermet *et al.* and Ravinski *et al.*<sup>23,24</sup> In the BFO system spectra, some unassigned modes, identified as little arrows, could belong to the phonons of the spurious phase  $\text{Bi}_{25}\text{FeO}_{40}$  present in this sample.

The modes in the region up to  $167\text{ cm}^{-1}$  are dominated by the relative motion of the Bi ions respect to  $\text{FeO}_6$  octahedra, while the modes above are mainly dominated by oxygen

motion.<sup>23,25</sup> The principal changes in the Raman spectra features of the studied samples are concentrated in the first region, below  $167\text{ cm}^{-1}$ . The modes labeled as E(TO1) and E(TO2) shift to lower frequencies (red shift) with dopant incorporation ( $73\text{ cm}^{-1}$  and  $139\text{ cm}^{-1}$  for BFO,  $68\text{ cm}^{-1}$  and  $133\text{ cm}^{-1}$  for BBFT and  $68\text{ cm}^{-1}$  and  $135\text{ cm}^{-1}$  for BBLFT, respectively). In simple harmonic model, the frequency is given by  $\omega^2 = k/m^*$ , being  $k$  the force constant and  $m^*$  the reduced mass of the oscillator systems. According to this equation, the E(TO1) and E(TO2) should shift to higher frequencies (blue shift) due to the decrease in the reduced mass induced for dopant incorporation (Bi ion is heavier than Ba and La ions). Hence, the red shift experimented by this two modes is related to a huge softening of the force constant  $k$  between  $\text{A}_{\text{sites}}\text{-O}$  bonds, strong enough to overcome the

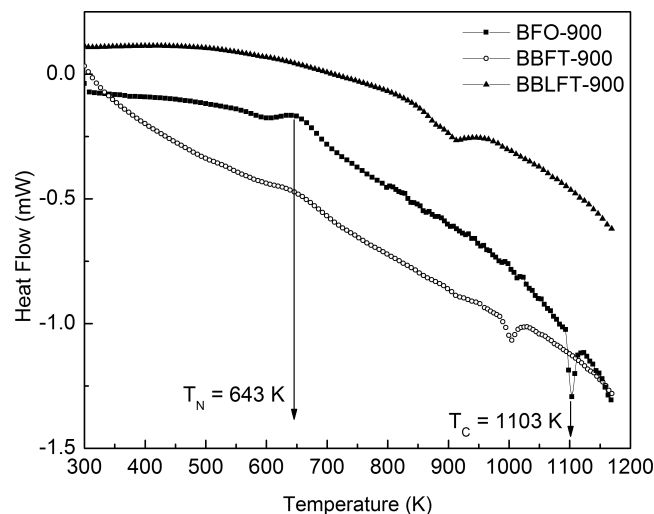


Fig. 3. DSC of all samples.

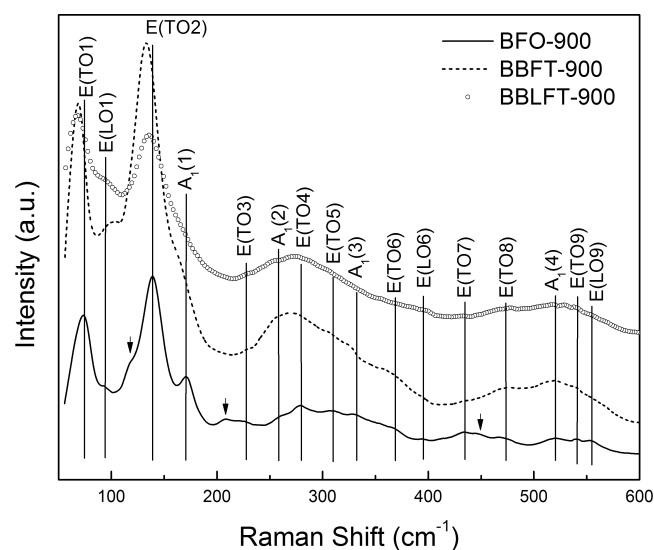


Fig. 4. Raman spectra of the samples.

blue shift that would introduce the reduction in  $m^*$ . The weakening of the strong hybridization between Bi and O due to dopant incorporation, agree well with the reduction in ferroelectric transition temperature observed.

The magnetic properties of the studied ceramics are shown in Fig. 5. The hysteresis loops at room temperature and 5 K are presented in Fig. 5(a). Not hysteretic behavior is observed in bulk BFO-900 system, typical antiferromagnetic linear dependence of  $M$  versus  $H$  at room temperature is in agreement with other reports published previously.<sup>22,26,27</sup> For the doped samples, a weak ferromagnetic behavior with typical hysteresis loop and enhanced magnetic properties compared to the undoped BFO-900 is observed. Similar improvement of magnetic properties had been reported earlier for doped BFO system.<sup>12,28–30</sup>

The magnetization at the highest field applied  $\sigma_{3T}$  ( $H = 3T$ ) increase from 0.12 emu/g for the undoped system to 0.37 emu/g and 0.56 emu/g for the BBFT-900 and the BBLFT-900, respectively. The remnant magnetization  $\sigma_r$  is similar and around 0.09 emu/g for doped samples, while the coercive field  $iH_c$  decrease with dopant incorporation from 2270 Oe for BBFT-900 to 850 Oe for BBLFT-900. At low temperature (5 K, inset in Fig. 5(a)) similar ferromagnetic behavior with a slight increase of the  $\sigma_{3T}$  and slight decrease in  $iH_c$  compared to room temperature is observed in doped samples. These changes in  $\sigma_{3T}$  and  $iH_c$  obeys to the reduction of thermal motion at low temperature. The fact that the system did not restore the antiferromagnetic nature of BFO is a clear evidence of the suppression of the spiral spin structure and confirms the ferromagnetic order of the doped samples. Furthermore, the shape of the loop, in which no saturation tendency exist (measurements up to 6 T shows the same behavior, no shown here) and the low magnetization achieved suggest the stabilization of a canted spin structure.

Figure 5(b) shows the low temperature field cooling magnetic dependency of the BBFT-900 and BBLFT-900. Even when the bias field is above the coercive one, no continuous increase of the magnetization during cooling, as expected,<sup>25,31–33</sup> is observed. The magnetization passes through a maximum around 92 K and then decrease to a value above that of room temperature. This anomaly could be a consequence of a spin reorientation due to a drastic change in the anisotropy constant around that temperature. Further studies of the role of anisotropy in the magnetic order of BFO-based system are needed.

In the literature, the suppression or frustration of the spatially modulated spin structure, due to the oxygen vacancies and/or the coexistence of  $Fe^{2+}$  and  $Fe^{3+}$  ( $Fe^{3+}-O^{2-}-Fe^{2+}$  double exchange interactions), is ascribed generally as the cause of the weak ferromagnetism developed in BFO-based system.<sup>27,34</sup> To understand and clarify the origin of the observed magnetic behavior, the XPS of the samples was investigated. The XPS narrow scan spectra of Fe 2p, O 1s and Bi 4f are presented in Fig. 6.

The  $2p_{1/2}$  and  $2p_{3/2}$  splitting of Fe 2p core level is presented in Fig. 6(a). The coexistence of two valence state for Fe ( $Fe^{2+}$  and  $Fe^{3+}$ ) was confirmed from the Gaussian deconvolution of the spectra. To accurate account, the two contributions and the contribution of the satellite peaks, all the spectra was fitted (dashed and solid lines, only shown for BFO-900 for clarity). The results reveals the presence of the two valence state for all the studied samples, being the  $Fe^{3+}$  to  $Fe^{2+}$  ratio 62/38, 56/44 and 59/41 for BFO-900, BBFT-900 and BBLFT-900, respectively. Similar  $Fe^{3+}/Fe^{2+}$  values have been reported in the literature.<sup>34</sup> No tendency can be identified with dopant incorporation. Its worth to note that in the case of undoped sample, the  $Fe^{3+}$  to  $Fe^{2+}$  ratio could be slightly affected by the presence of the impurity phase detected.

The O 1s XPS spectrum (Fig. 6(b)) is an asymmetric peak due to the overlap of two contributions (solid lines are only

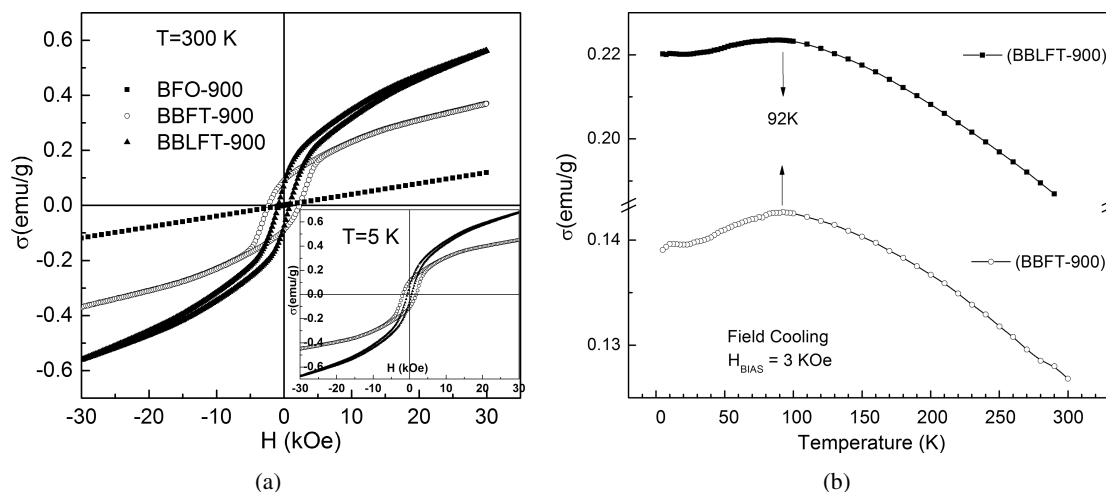


Fig. 5. (a) Magnetic hysteresis loops and (b) low temperature dependence of magnetization.

guide to the eyes). One main narrow peak around  $529 \text{ cm}^{-1}$ – $529.5 \text{ cm}^{-1}$  that can be associated with the of O 1s binding energy. Another wide peak, observed for all the samples at higher energies as a shoulder of the main peak, can be associated to oxygen defects.<sup>32</sup> As the electric neutrality is consider in the nominal composition, the formation of oxygen vacancies is due to the reduction of the  $\text{Fe}^{3+}$  to  $\text{Fe}^{2+}$ .

The inset in Fig. 6(b), shows the  $4f_{5/2}$  and  $4f_{7/2}$  splitting of the Bi 4f core level. For BFO-900 the binding energies are  $163.8 \text{ cm}^{-1}$  ( $4f_{5/2}$ ) and  $158.5 \text{ cm}^{-1}$  ( $4f_{7/2}$ ). For the doped samples, these peaks shift to lower energies (around  $163.4 \text{ cm}^{-1}$  ( $4f_{5/2}$ ) and  $158 \text{ cm}^{-1}$  ( $4f_{7/2}$ )). This doublet is mainly identified as a signal from Bi–O bonds in the perovskite structure. Hence, the shift to lower energies indicates a weakening of Bi–O bonds, in complete agreement with the results obtained from Raman spectroscopy. Two extra peaks below the main ones can be observed in the BFO-900 spectra

that can be associated with Bi-rich spurious phase detected from XRD. The Gaussian deconvolution of the spectra (solid lines) reveals that the  $\text{Bi}_{25}\text{FeO}_{40}$  content is around a 7.5%, very close to the 5% obtained from XRD analysis, considering the difference between the two techniques.

As can be noted from the above results, in all the studied samples the coexistence of the Fe in two valence states and the presence of oxygen vacancies is confirmed. Suggesting that, the improvement of magnetic properties of doped samples is not a direct consequence of oxygen vacancies and/or the coexistence of  $\text{Fe}^{2+}$  and  $\text{Fe}^{3+}$  because the same scenario is present in both, doped and undoped ones. Combining the results from XRD, Raman and XPS analysis it may be concluded that the enhancement of magnetic properties could be due to reduction of the rhombohedral distortion and weakening of the Bi–O bonds. These changes affects directly the length and the angles between neighboring magnetic

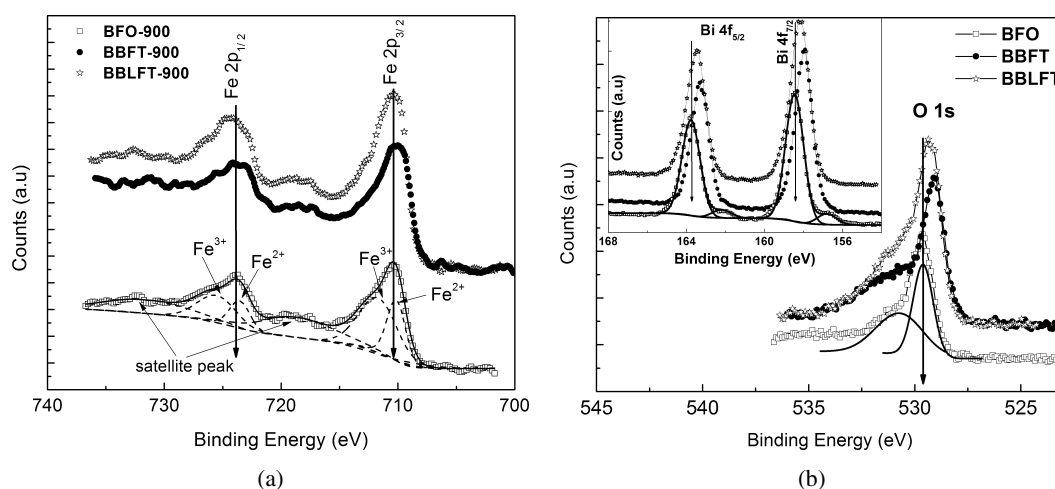


Fig. 6. XPS narrow scan spectra for the studied samples (a) Fe 2p and (b) O 1s (Bi 4f in the inset).

elements and therefore, change the strength of the super exchange and double exchange interaction  $\text{Fe}^{3+}\text{-O-Fe}^{3+}$  and  $\text{Fe}^{3+}\text{-O-Fe}^{2+}$ , respectively. The change induced in magnetic interactions suggest an effective suppression of the spatially modulated spin structure and to the stabilization of a canted spin structure in doped samples.

#### 4. Conclusions

BFO and doped BFO bulk ceramic have been prepared by solid state reaction route. The XRD results confirm that the dopant incorporation improve the BFO rhombohedral phase stability. In the case of the undoped system, a minority residual Bi-rich phase (around 5%) was detected. A reduction of the rhombohedral distortion, introduced by the lone pair  $6s^2$  of the  $\text{Bi}^{3+}$  and a decrease in grain size with dopants incorporation was detected as well.

The enhancement of magnetic properties in doped samples was attributed to the reduction of the rhombohedral distortion and weakening of the Bi–O bonds rather than the coexistence of  $\text{Fe}^{2+}$  and  $\text{Fe}^{3+}$  and/or the presence of oxygen vacancies established via XPS measurements. Finally, the weakening of the Bi–O bonds, confirmed by XPS and Raman experiments, conduce to a continuous decrement of the ferroelectric-paraelectric transition temperature.

#### Acknowledgments

The authors wish to thank to ICTP for financial support of the Latin-American Network of Ferroelectric Materials (NET-43). The authors also wish to thank CINVESTAV, Unidad Querétaro, for infrastructure facilities and auxiliars Ing. José Alfredo Muñoz Salas, Ing. José Eleazar Urbina Alvarez, Ing. Francisco Rodríguez Melgarejo and I. Q. María Carmen Delgado Cruz for XPS, SEM, Raman and DSC measurements, respectively. Dr. Osmany García and Dr. Francisco Calderón wish to thank CONACYT for financial support of the Projects 262041 and 262126, respectively.

#### References

- <sup>1</sup>J. F. Tressler, S. Alcoy and R. E. Newnhan, Piezoelectric sensors and sensor materials, *J. Electroceram.* **2**(4), 257 (1998).
- <sup>2</sup>B. Jaffe and W. Cook, *Piezoelectric Ceramics* (Academic Press, 1971).
- <sup>3</sup>H. G. Haertling, Ferroelectric ceramics: History and technology, *J. Am. Ceram. Soc.* **82**(4), 797 (1999).
- <sup>4</sup>N. A. Spaldin, *Magnetic Materials: Fundamentals and Applications*, 2nd edn. (Cambridge University Press, 2011).
- <sup>5</sup>N. A. Pertsev and H. Kohlstedt, Resistive switching via the converse magnetoelectric effect in ferromagnetic multilayers on ferroelectric substrates, *Nanotechnology* **21**, 475202 (2010).
- <sup>6</sup>R. K. Gupta, K. Ghosh and P. K. Kahol, Room temperature ferromagnetic multilayer thin film based on indium oxide and iron oxide for transparent spintronic applications, *Mater. Lett.* **64**, 2022 (2010).

- <sup>7</sup>G. Xu, J. Wen, C. Stock and P. M. Gehring, Phase instability induced by polar nanoregions in a relajador ferroelectr. system, *Nature Mater.* **7**, 562 (2008).
- <sup>8</sup>H. N. Tailor, A. A. Bokov and Y. Zuo-Guang, Dielectric characterization of  $(1-x)\text{PMN-xPT}$  ( $x=0.07$  and  $0.10$ ) ceramics synthesized by an ethylene glycol-based soft chemical route, *IEEE Trans. Ultrason. Ferroelectr. Freq. Control* **58**(9), 1920 (2011).
- <sup>9</sup>K. H. J. Buschow and F. R. Boer, *Physics of Magnetism and Magnetic Materials* (Kluwer Academic Publishers, 2004).
- <sup>10</sup>C. Shang-Jui, L. Yen-Ting, Y. Ge-Ping, L. Hsin-Yi and H. Jia-Hong, The structure and ferroelectric property of La-doped  $\text{BiFeO}_3/\text{SrTiO}_3$  artificial superlattice structure by rf sputtering: Effect of deposition temperature, *Thin Solid Films* **529**, 85 (2013).
- <sup>11</sup>D. H. Wang, W. C. Goh, M. Ning and C. K. Ong, Effect of Ba doping on magnetic, ferroelectric, and magnetoelectric properties in multiferroic  $\text{BiFeO}_3$  at room temperature, *Appl. Phys. Lett.* **88**, 212907 (2006).
- <sup>12</sup>D. Varshney, A. Kumar and K. Verma, Effect of A site and B site doping on structural, thermal, and dielectric properties of  $\text{BiFeO}_3$  ceramics, *J. Alloys Compd.* **509**, 8421 (2011).
- <sup>13</sup>J. Silva, A. Reyes, H. Esparza, H. Camacho and L. Fuentes,  $\text{BiFeO}_3$ : A review on synthesis, doping and crystal structure, *Integr. Ferroelectr.* **126**, 47 (2011).
- <sup>14</sup>V. E. Wood and A. Austin, Possible applications for magnetoelectric materials, *Int. J. Magn.* **5**, 303 (1974).
- <sup>15</sup>N. A. Hill, Why are there so few magnetic ferroelectrics?, *J. Phys. Chem. B* **104**, 6694 (2000).
- <sup>16</sup>R. Y. Zheng, X. S. Gao, Z. H. Zhou and J. Wang, Multiferroic  $\text{BiFeO}_3$  thin films deposited on  $\text{SrRuO}_3$  buffer layer by rf sputtering, *J. Appl. Phys.* **101**, 054104 (2007).
- <sup>17</sup>M. Y. Shami, M. S. Awan and M. Anis-ur-Rehman, Phase pure synthesis of  $\text{BiFeO}_3$  nanopowders using diverse precursor via coprecipitation method, *J. Alloys Compd.* **509**, 10139 (2011).
- <sup>18</sup>I. Sosnowska, T. P. Neumaier and E. Streichele, Spiral magnetic ordering in bismuth ferrite, *J. Phys. Chem.* **15**, 4835 (1982).
- <sup>19</sup>Q. Hang, Z. Xing, X. Zhu, M. Yu, Y. Song, J. Zhu and Z. Liu, Dielectric properties and related ferroelectric domain configurations in multiferroic  $\text{BiFeO}_3\text{-BaTiO}_3$  solid solutions, *Ceram. Int.* **38S**, S411 (2012).
- <sup>20</sup>T. Wang, C. Tu, Y. Ding, T. Lin, C. Ku, W. Yang, H. Yu, K. Wu, Y. Yao and H. Lee, Phase transition and ferroelectric properties of  $x\text{BiFeO}_3\text{-(1-x)BaTiO}_3$  ceramics, *Cur. Appl. Phys.* **11**, S240 (2011).
- <sup>21</sup>C. Yang, J. Ji-Sen, Q. Fang-Zhen, D.-M. Jiang, W. Chun-Mei and Z. Wei-Guo, Effect of Ba doping on magnetic and dielectric properties of nanocrystalline  $\text{BiFeO}_3$  at room temperature, *J. Alloys Compd.* **507**, 29 (2010).
- <sup>22</sup>S. Díaz-Castañón, O. García-Zaldívar, J. Faloh-Gandarilla, B. E. Watts, F. Calderón-Piñar, M. A. Hernández-Landaverde and F. J. Espinoza-Beltran, Synthesis of powders and thin films of bismuth ferrite from solution: A magneto-electric study, *Appl. Phys. A* **117**(3), 1283 (2014).
- <sup>23</sup>P. Hermet, M. Goffinet, J. Kreisel and P. Ghosez, Raman and infrared spectra of multiferroic bismuth ferrite from first principles, *Phys. Rev. B* **75**, 220102(R) (2007).
- <sup>24</sup>A. F. Ravinski, V. V. Triguk and I. I. Makoed, *Ab initio* calculations of the lattice dynamics and the ferroelectric instability of the  $\text{BiFeO}_3$  multiferroic, *Phys. Solid State* **56**(9), 1799 (2014).
- <sup>25</sup>J. Bielecki, P. Svedlindh, D. T. Tibebe, S. Cai and E. Sten-G., Structural and magnetic properties of isovalently substituted

- multiferroic BiFeO<sub>3</sub>: Insights from Raman spectroscopy, *Phys. Rev. B* **86**, 184422 (2012).
- <sup>26</sup>R. Das and K. Mandal, Magnetic, ferroelectric and magnetoelectric properties of Ba-doped BiFeO<sub>3</sub>, *J. Magn. Mater.* **324**, 1913 (2012).
- <sup>27</sup>H. Wu, Y. B. Lin, J. J. Gong, F. Zhang, M. Zeng, M. H. Qin, Z. Zhang, Q. Ru, Z. W. Liu, X. S. Gao and J. M. Liu, Significant enhancements of dielectric and magnetic properties in Bi(Fe<sub>1-x</sub>Mgx)O<sub>3-x/2</sub> induced by oxygen vacancies, *J. Phys. D, Appl. Phys.* **46**, 145001 (2013).
- <sup>28</sup>H. Deng, M. Zhang, Z. Hu, Q. Xie, Q. Zhong, J. Wei and H. Yan, Enhanced dielectric and ferroelectric properties of Ba and Ti co-doped BiFeO<sub>3</sub> multiferroic ceramics, *J. Alloys Compd.* **582**, 273 (2014).
- <sup>29</sup>A. Gautam and V. Rangra, Effect of Ba ions substitution on multiferroic properties of BiFeO<sub>3</sub> perovskite, *Cryst. Res. Technol.* **45**, 953 (2010).
- <sup>30</sup>P. Priyadharsini, A. Pradeep, B. Sathyamoorthy and G. Chandrasekaran, Enhanced multiferroic properties in La and Ce co-doped BiFeO<sub>3</sub> nanoparticles, *J. Phys. Chem. Solids* **75**, 797 (2014).
- <sup>31</sup>Q. Xu, X. Zheng, Z. Wen, Y. Yang, D. Wu and M. Xu, Enhanced room temperature ferromagnetism in porous BiFeO<sub>3</sub> prepared using cotton templates, *Solid State Commun.* **151**, 624 (2011).
- <sup>32</sup>L. Fang, J. Liu, S. Ju, F. Zheng, W. Dong and M. Shen, Experimental and theoretical evidence of enhanced ferromagnetism in sonochemical synthesized BiFeO<sub>3</sub> nanoparticles, *Appl. Phys. Lett.* **97**, 242501 (2010).
- <sup>33</sup>L. Bing-Cheng, C. Chang-Le and J. Ke-Xin, Low temperature properties of multiferroic BiFe<sub>0.9</sub>Cr<sub>0.1</sub>O<sub>3</sub> compound, *Solid State Commun.* **151**, 712 (2011).
- <sup>34</sup>G. Dong, G. Tan, Y. Luo, W. Liu, H. Ren and A. Xia, Optimization of the multiferroic BiFeO<sub>3</sub> thin films by divalent ion (Mn, Ni) co-doping at B-sites, *Mater. Lett.* **118**, 31 (2014).